Journal Name

Full Paper

Engineered Exciton Diffusion Length Enhances Device Efficiency in Small Molecule Photovoltaics

Received 00th January 20xx,
Accepted 00th January 20xx

DOI: 10.1039/x0xx00000x

www.rsc.org/

*Muhammad T. Sajjad,† Oskar Blaszczyk,† Lethy Krishnan Jagadamma, Thomas J. Roland, Mithun Chowdhury, Arvydas Ruseckas, Ifor D. W. Samuel**

In organic photovoltaic blends, there is a trade-off between exciton harvesting and charge extraction because of the short exciton diffusion length. Developing a way of increasing exciton diffusion length would overcome this trade-off by enabling efficient light harvesting from large domains. In this work, we engineered (enhanced) both exciton diffusion length and domain size using solvent vapour annealing (SVA). We show that SVA can give a three-fold enhancement in exciton diffusion coefficient (D) and nearly a doubling of exciton diffusion length. It also increases the domain size, leading to enhancement of charge extraction efficiency from 63 to 89%. Usually larger domains would reduce exciton harvesting but this is overcome by the large increase in exciton diffusion, leading to a 20% enhancement in device efficiency.

Introduction

Organic photovoltaics (OPVs) are a promising solar technology because of their great potential to give lightweight, flexible and low-cost solar cells. Devices with power conversion efficiency (PCE) of more than 10% are being regularly reported using bulk heterojunction (BHJ) device architectures.[1-3] Further device improvement requires the optimization of phase separation between electron donor and acceptor. The length scale of phase separation influences both exciton harvesting (charge generation) and charge extraction. Charge generation occurs at the interface between the electron donor and acceptor, and for efficient exciton harvesting the donor and acceptor domain sizes should be smaller than the exciton diffusion length (L_D) which is typically rather short, below 10 nm.[4,5] The small domains give a large surface area which assists exciton harvesting, but also enhances charge recombination.[5] This means that for a given exciton diffusion length, as domain size is varied there is a trade-off between exciton harvesting and charge extraction. Developing a way of increasing exciton diffusion length would overcome this trade-off by enabling efficient light harvesting from large domains, which would then also give improved charge extraction and therefore reduced recombination.

Several methods have been used to optimize domain sizes and morphology of OPV blends, including thermal and solvent annealing, and the use of high-boiling-point additives. The resulting improvements in device performance have been attributed to increased domain size and crystallinity and/or better miscibility of donor and acceptor molecules.[6-11] Compared to the attention given to morphology optimization, little work has been done to enhance exciton diffusion. There are a few reports where exciton diffusion length was enhanced using different processing techniques like thermal annealing[12-14] and solvent vapour annealing[13], and diluting molecules in a host matrix to enhance exciton lifetime [15]. The last of these enhanced L_D and so increased power conversion efficiency in planar heterojunction solar cells to 4.4% which is 30% higher than that of control cells made using undiluted molecules.[15] However, to the best of our knowledge, improved photovoltaic performance in bulk heterojunctions by engineered exciton diffusion has not been demonstrated.

Here we show that solvent vapour annealing (SVA) can be used to increase the exciton diffusion length and also to increase domain size. This engineered increase of the exciton diffusion length in combination with the larger domain size leads to efficient light harvesting and charge extraction, and hence a substantial (20%) increase in device efficiency. For this we employed a range of different solvents and systematically investigated their effect on exciton diffusion in two efficient thiophene based small molecules DR3TBDTT[16] and SMPV1[17]. In both molecules, carbon disulfide (CS_2) shows the most promising results, with more than three-fold enhancement in exciton diffusion coefficient (D) and two-fold enhancement in exciton diffusion length. The optimized CS_2 annealed devices consistently show a PCE between 7.0 and 7.7%, and a charge extraction efficiency above 80% at short circuit conditions

Organic Semiconductor Centre, SUPA, School of Physics & Astronomy, North Haugh, St Andrews, KY16 9SS, United Kingdom

† MTS and OB contributed equally to this work.

Electronic Supplementary Information (ESI) available: The absorption and photoluminescence (PL) spectra of neat donor molecules, exciton-exciton annihilation measurements, device characteristics of SMPV1:$PC_{71}BM$ blends, as well as measurements of charge generation, blend morphology and optical constants. See DOI: 10.1039/x0xx00000x

which is enabled by a large average domain size of about 30 nm. Large domain size would normally reduce exciton harvesting but in our case higher device efficiency is obtained because of the increase in exciton diffusion length.

Results and discussion

The molecular structure of DR3TBDTT[16] (containing a central alkoxy-substituted benzo[1,2-b:4,5-b']dithiophene (BDT) unit) and SMPV1[17] (with BDT-T as the core unit and 3-octylrodanine as the electron-with-drawing end-group) are shown in Fig. 1a and 1b. Three different solvents; tetrahydofuran (THF), chloroform ($CHCl_3$) and carbon disulfide (CS_2) with a range of boiling points were used for annealing the films. For both molecules, the annealing conditions for each solvent were optimised to maximise enhancement of the absorption coefficient which was determined using spectroscopic ellipsometry (Fig. S1a and S1b).

After the optimisation of the SVA conditions, we investigated their effect on exciton diffusion which we measured using singlet-singlet exciton annihilation. This was done by measuring time-resolved photoluminescence (TRPL) decays at different excitation densities which are given in Fig. S2 and S3. PL decays get faster at high excitation densities because excitons are closer to each other and annihilate more often. The PL intensity is proportional to exciton density *N* which can be described by a rate equation[13, 18]

$$\frac{dN}{dt} = G - kN - \gamma N^2 \qquad (1)$$

where *G* is for exciton generation which is instantaneous in this case, *k* is the decay rate constant in the absence of annihilation and $\gamma(t)$ is the annihilation rate constant which for a diffusion-limited annihilation in a three-dimensional isotropic system can be described by sum of a time-independent term and a time-dependent term[13]

$$\gamma(t) = 4\pi R_a D \left(1 + \frac{R_a}{\sqrt{2\pi D t}}\right) \qquad (2)$$

where *D* is the exciton diffusion coefficient and R_a is the annihilation radius. We simulated γ(t) in the form of Equation 2 and fitted the intensity-dependent PL decays using Equation 1. The results are shown in Fig. 1c and 1d. For R_a we used the previously reported d_{100}-spacing value of 2.04 nm and 2.11 nm for DR3TBDTT[10] and SMPV1[17] respectively. The resulting values of diffusion coefficients are shown in Fig. 1e. In both molecules, D increases after SVA with the largest increase for CS_2 where D triples for DR3TBDTT and doubles for SMPV1. This enhancement in D after SVA is due to improved crystallinity of SVA films.[10, 13, 22]

We determined the three-dimensional exciton diffusion length which is most relevant to bulk heterojunctions using[14]

$$L_{3D} = \sqrt{6D\tau} \qquad (3)$$

where τ is the lifetime in the absence of annihilation. The obtained L_{3D} for both molecules with and without SVA are shown in Fig. 1f. Untreated films of DR3TBDTT have a significantly higher value of L_{3D} (25 nm) compared to untreated SMPV1 (~7 nm) which can be attributed to the higher crystallinity of DR3TBDTT.[10] For both molecules there is little change in PL lifetime after SVA, and so the increase in D also leads to an increase in L_{3D}. The enhancement in L_{3D} strongly depends on the nature of the solvent used for treatment. For example the highest improvement is seen for the solvent with the lowest boiling point (CS_2) where L_{3D} is doubled and the lowest improvement is seen for the solvent with the high boiling point (THF) for both molecules.

To investigate the effect of processing conditions and exciton diffusion on device performance, we made solar cells using blends of both molecules (DR3TBDTT and SMPV1) with $PC_{71}BM$. For each case (DR3TBDTT or SMPV1), we fabricated two sets of devices; one blend without SVA and one blend treated with the best protocol SVA with CS_2. The device characteristics of DR3TBDTT:$PC_{71}BM$ blends before and after SVA are shown in Fig. 2 and the corresponding results for SMPV1:$PC_{71}BM$ are shown in Fig. S5. The solar cell device efficiencies reported in the present work are comparable to previously reported values using simple device architecture of ITO/PEDOTPSS/active layer/Ca or LiF/Al. For example PCEs of 4.83%[22] and 7.2%[17] were obtained for SMPV1:$PC_{71}BM$ blend and 6.92%[23] for DR3TBDTT:$PC_{71}BM$ blends in chloroform. Furthermore our solar cell device efficiencies are around 80 % of the record efficiency values reported for these molecules in a more complicated device.[10,17] We used the most commonly used simple device architecture of ITO/PEDOTPSS/active layer/Ca/Al whereas in the previous reports they used additives such as PDMS (for SMPV1:$PC_{71}BM$)[17] and special electron transport layers such as $PrC_{60}MA$ (for DR3TBDTT:$PC_{71}BM$)[10] to obtain higher efficiency.

Illuminated current density-voltage (J-V) curves of optimised blends of both molecules with $PC_{71}BM$ (Fig. 2a and S5a) clearly show the enhancement in the short-circuit current after CS_2 SVA. Similarly an enhancement in EQE and the absorption of optimised blends upon SVA was observed for both molecules. Furthermore, the absorption spectra of SVA blends show that the strong peak of DR3TBDTT and SMPV1 is red-shifted compared to their untreated blends. This shift is more in the case of DR3TBDTT where approximately 20, 16 and 10 nm red-shift was seen for CS_2, $CHCl_3$ and THF compared to SMPV1 where only 2 to 5 nm shift was seen. Furthermore, this strong absorption peak becomes stronger upon SVA for both molecules. However, this enhancement is larger for the case of DR3TBDTT:$PC_{71}BM$ blend which shows better order packing and increased conjugation length compared to SMPV1:$PC_{71}BM$ blend after solvent annealing.[10]

The internal quantum efficiency (IQE) of DR3TBDTT and SMPV1 based solar cells determined from optical modelling of the device stacks (detail given in Supplementary Information) are given in Fig. 2d and S5d respectively. The enhancement in IQE upon SVA shows that the improvement in devices is not only due to absorption enhancement but also the absorbed photons are converted into charges more efficiently. The photovoltaic parameters of devices for both molecules before and after SVA are given in Table 1. For both molecules, SVA devices shows higher J_{sc} and FF whereas a small drop in V_{oc} was seen**.** The increased J_{sc} is due to a combined effect of improved absorption and enhanced charge extraction at short circuit conditions, whereas improved FF indicates better charge transport

at low built-in electric field possibly because of improved percolation pathways and higher charge mobility. The decrease in V_{oc} can be related to the observed redshift in the absorption spectra of the SVA blend films in the wavelength region (750-800 nm). Since this band edge mainly corresponds to the donor molecules, this shift indicates that in SVA blend films, there is an increase in conjugation length due to an improved planarization of the donor molecule aggregates, which will further contribute to the increased inter-chain interaction between the donor molecules.[19] Overall the devices of DR3TBDTT and SMPV1 with CS_2 SVA showed 24% and 8% enhancement in average PCE compared to their untreated blends respectively.

To understand the mechanism of improved photovoltaic performance by SVA, we investigated charge generation using transient absorption (TA) spectroscopy. We used an excitation wavelength of 630 nm at which there is no contribution to the TA signal from the $PC_{71}BM$ absorption. First we measured the TA spectra of neat donor films (without $PC_{71}BM$) which did not change with time after excitation implying that singlet excitons are the only species generated (Fig. S6a and S6b). Using the known excitation density, sample thickness and absorbance we determined the absorption cross section of the exciton as a function of wavelength (Fig. S7a and S7b). Then the TA spectra of the blends with $PC_{71}BM$ were measured (Fig. S8). By subtracting the exciton contribution to TA spectra at early times and assuming that each photon absorbed generates an exciton or charge pair we obtain the charge pair absorption spectrum as a function of wavelength (Fig. S7a and S7b). We have built a kinetic model to describe the conversion dynamics of singlet excitons into charges and charge recombination (Fig. S9), and performed a global analysis to fit the experimental TA spectra with this model. The obtained dynamics of excitons and charges in DR3TBDTT: $PC_{71}BM$ blends are given in Fig. 3a. It shows that in the untreated DR3TBDTT:$PC_{71}BM$ blend about 27% of charge pairs are generated within 200 fs after excitation. The remaining 73% are generated in the following 100 ps by excitons diffusing to the heterojunction. The total charge generation efficiency $\Phi_{gen} = 0.93$ in the untreated blend is obtained from the global fit. In the blend after CS_2 SVA only 20% of charge pairs are generated in 200 fs with the remaining 80% generated in the following 200 ps. Slower charge generation after SVA compared to the untreated blend suggests that domain sizes of the donor increase upon SVA. Because excitons move by incoherent hopping, it takes longer for them to reach the interface between donor and acceptor in larger domains and to split into charge pairs. This is supported by AFM images which show an increase in feature size as well as an increase in the surface roughness upon SVA in CS_2 (Fig. 3b and 3c). Despite slow charge generation in CS_2 SVA blend $\Phi_{gen} = 0.74$ is only slightly lower than in the untreated blend. This is due to the large exciton diffusion length which enables the excitons to reach a heterojunction in their lifetime. Slower charge generation after SVA is also observed in SMPV1: $PC_{71}BM$ blend (results are shown in Fig. S11). The charge generation efficiency in the untreated SMPV1 blend is $\Phi_{gen} = 0.88$ and decreases to $\Phi_{gen} = 0.71$ in the CS_2 SVA blend.

The internal quantum efficiency (IQE) is the product of charge generation efficiency Φ_{gen} and charge extraction efficiency Φ_{extr} at short circuit conditions $\mathrm{IQE} = \Phi_{gen}\Phi_{extr}$. Using Φ_{gen} obtained from TA spectroscopy at 630 nm excitation wavelength and IQE from optical modelling of the device stacks at the same wavelength (details given in experimental method) we estimate that Φ_{extr} increases from 0.63 in untreated blend to 0.89 after CS_2 SVA. Similarly, in SMPV1:$PC_{71}BM$ blends Φ_{extr} increases from 0.59 to 0.80. The increase in charge extraction efficiency can be explained by larger domains after SVA. The average domain size of electron acceptor can be estimated from the diffusion-limited PL quenching in the blends. The PL decays in neat DR3TBDTT and in blends with $PC_{71}BM$ are shown in Fig. 3d. Blends show faster PL decay compared to neat film due to exciton dissociation at the heterojunction. We extracted the average size of $PC_{71}BM$ domains by considering that PL quenching is limited by exciton diffusion[20] (details given in supplementary information) and the results are plotted in Fig. 3e. For the DR3TBDTT:$PC_{71}BM$ blend the fullerene domain size increased from 9 nm to about 34 nm with CS_2 SVA. Similarly, for SMPV1:$PC_{71}BM$ blends the average domain size increased from 5 nm to about 31 nm with CS_2 SVA. The increase of domain size is consistent with AFM images and with a previous report where an enhancement in the phase separation upon CS_2 solvent vapour annealing was seen from analysis of TEM phase images for the case of DR3TBDTT: $PC_{71}BM$ blend.[10] The cross-sectional TEM images of pristine and SVA blends show that donor and acceptor domains are distributed homogeneously in these blends without noticeable vertical phase separation (Figure S14). In Fig. 3f we plot charge extraction efficiency as a function of average domain size and find a direct correlation between them, indicating that larger domains support more efficient charge extraction.

Conclusion

We investigated the problems of short L_D and domain size, and enhanced them to improve OPV efficiency in two highly efficient small molecules using solvent vapour annealing. We explored the effect of a range of solvents and observed significant enhancement (up to 3 times) in exciton diffusion coefficient and a doubling of exciton diffusion length for both molecules. We then fabricated organic solar cells using this approach and found an enhancement in PCE in the optimized CS_2 SVA devices. Our results show that SVA increases exciton diffusion length and domain size. This means that exciton harvesting is still efficient even in larger domains which lead to improved charge extraction and hence higher solar cell efficiencies.

Experimental Section

Exciton diffusion and PL quenching measurements: Materials for this study were purched from 1-Material. Fluorescence decays of neat and blend films were measured using a Hamamatsu C6860 synchroscan streak camera. The films were excited using ~ 200 fs pulses at 515 nm with 80 MHz repetition rate. For exciton-exciton annihilation measurements on neat films, an excitation wavelength of 590 nm and a repetition rate of 100 kHz were used.

Transient absorption spectroscopy: The measurement was performed using the HARPIA spectrometer from Light Conversion. The films were excited using ~ 200 fs pump pulses at 630 nm with 50 kHz repetition rate from a PHAROS regenerative amplifier (Light

Conversion). For probe a white light continuum was used which was generated using a sapphire plate.

Device fabrication and characterisation: The organic solar cell device architecture used in this study is glass/ITO/PEDOT:PSS/ DR3TBDTT or SMPV1:$PC_{71}BM$ /Ca/Al. The active layer solution was prepared by keeping the donor concentration (for both SMPV1 and DR3TBDTT) of 14 mg/ml and the donor: acceptor ratio of 1:0.8 in Chloroform solvent. For solvent vapor annealing experiment, 150-200 uL of CS_2 solvent was gently dripped through the edges of a glass petri-dish with diameter of ~ 10 cm and the active layer film was kept inside for ~ 45 seconds with the lid closed. Ca (7 nm) and Al (100 nm) were thermally evaporated using a shadow mask. The active area of the devices was 0.08 cm^2 (4 mm × 2 mm).

After the electrode deposition, the devices were encapsulated with a UV optical adhesive and a glass coverslip. The current–voltage characteristics were determined using a Sciencetech solar simulator and a Keithley 2400 source-measure unit. The illumination intensity was verified with a calibrated monosilicon detector and a KG-5 filter. The external quantum efficiency (EQE) measurements were performed at zero bias by illuminating the device with monochromatic light supplied from a Xenon arc lamp in combination with a dual-grating monochromator. The number of photons incident on the sample was calculated for each wavelength by using a silicon photodiode calibrated by the National Physical Laboratory (NPL).

Atomic force microscopy: AFM was performed using the multimode 8 AFM unit from Bruker. The scans were done in tapping mode with a cantilever resonant frequency of 140 kHz.

Optical modelling: The refractive indexes of blends (with and without SVA) and PEDOT were measured using spectral ellipsometry and are given in Fig. S12. Literature values of refractive indexes of ITO, Ca and Al were used for optical modelling. The absorption simulations were preformed using transfer matrix[21] by taking into account all interference effects in the stack. Then IQE spectra were determined from EQE and 1-reflection.

Conflicts of interest

There are no conflicts to declare.

Acknowledgment

We acknowledge support from the European Research Council (grant 321305). IDWS acknowledges a Royal Society Wolfson Research Merit Award. We are grateful to EPSRC for equipment grant (EP/L017008/1) and for support of OB (EP/M508214/1). We are grateful to Dr David Miller for cross-sectional TEM. The research data supporting this publication can be accessed at http://dx.doi.org/10.17630/74e8277f-d1c7-4877-b515-d5ef8898733b.

Notes and references

1 S. Zhang, L. Ye and J. Hou, *Adv. Energy Mater.,* 2016, **6**, 1502529.
2 J. Zhao, Y. Li, G. Yang, K. Jiang, H. Lin, H. Ade, W. Ma and H. Yan, *Nature Energy,* 2016, ***1***, 15027.
3 L. Lu, T. Zheng, Q. Wu, A. M. Schneider, D. Zhao and L. Yu, *Chem. Rev.,* 2015, ***115***, 12666-12731.
4 O. V. Mikhnenko, P. W. Blom and T.-Q. Nguyen, *Energy Environ. Sci.,* 2015, **8**, 1867-1888.
5 G. J. Hedley, A. Ruseckas and I. D. W. Samuel, *Chem. Rev.,* 2017, ***117***, 796-837.
6 B. Walker, A. B. Tamayo, X. D. Dang, P. Zalar, J. H. Seo, A. Garcia, M. Tantiwiwat and T. Q. Nguyen, *Adv. Funct. Mater.,* 2009, ***19***, 3063-3069.
7 S. Jeong, S.-H. Woo, H.-K. Lyu and Y. S. Han, *Solar Energy Materials and Solar Cells,* 2011, ***95***, 1908-1914.
8 J. T. Rogers, K. Schmidt, M. F. Toney, E. J. Kramer and G. C. Bazan, *Adv. Mater.,* 2011, ***23***, 2284-2288.
9 Y. Sun, C. Cui, H. Wang and Y. Li, *Adv. Energy Mater.,* 2011, ***1***, 1058-1061.
10 M. Li, F. Liu, X. Wan, W. Ni, B. Kan, H. Feng, Q. Zhang, X. Yang, Y. Wang and Y. Zhang, *Adv. Mater.,* 2015, ***27***, 6296-6302.
11 G. J. Hedley, A. J. Ward, A. Alekseev, C. T. Howells, E. R. Martins, L. A. Serrano, G. Cooke, A. Ruseckas and I. D. W Samuel, *Nat. Commun.,* 2013, ***4, 2867***.
12 M. Sim, J. Shin, C. Shim, M. Kim, S. B. Jo, J.-H. Kim and K. Cho, *J. Phys. Chem. C,* 2014, ***118***, 760-766.
13 M. Chowdhury, M. T. Sajjad, V. Savikhin, N. Hergue, K. Sutija, S. Oosterhout, M. F. Toney, A. Ruseckas and I. D. W. Samuel, *Phys. Chem. Chem. Phys.,* 2017, **19**, 12441-12451.
14 Y. Long, G. J. Hedley, A. Ruseckas, M. Chowdhury, T. Roland, L. A. Serrano, G. Cooke and I. D. W. Samuel, *ACS Appl. Mater. Interfaces,* 2017, **9**, 14945-14952.
15 S. M. Menke, W. A. Luhman and R. J. Holmes, *Nat. Mater.,* 2013, ***12***, 152-157.
16 J. Zhou, Y. Zuo, X. Wan, G. Long, Q. Zhang, W. Ni, Y. Liu, Z. Li, G. He and C. Li, *J. Am. Chem. Soc.,* 2013, ***135***, 8484-8487.
17 Y. Liu, C.-C. Chen, Z. Hong, J. Gao, Y. M. Yang, H. Zhou, L. Dou, G. Li and Y. Yang, *Sci. Rep.,* 2013, ***3, 3356***.
18 P. E. Shaw, A. Ruseckas and I. D. W. Samuel, *Adv. Mater.,* 2008, ***20***, 3516-3520.
19 F. Panzer, H. Bässler, R. Lohwasser, M. Thelakkat and A. Köhler, *J. Phys. Chem. Lett.,* 2014, ***5***, 2742-2747.
20 A. Ruseckas, P. E. Shaw and I. D. W. Samuel, *Dalton Transactions,* 2009**,** (45), 10040-10043.
21 L. A. Pettersson, L. S. Roman and O. Inganäs, *J. Appl. Phys.,* 1999, ***86***, 487-496.
22 M. E. Farahat, C.-S. Tsao, Y.-C. Huang, S. H. Chang, W. Budiawan, C.-G. Wu and C.-W. Chu, *J. Mater. Chem. A, 2016,* **4**, 7341-7351.
23 J. Zhou, X. Wan, Y. Liu, Y. Zuo, Z. Li, G. He, G. Long, W. Ni, C. Li and X. Su, *J. Am. Chem. Soc.*, 2012, **134**, 16345-16351.

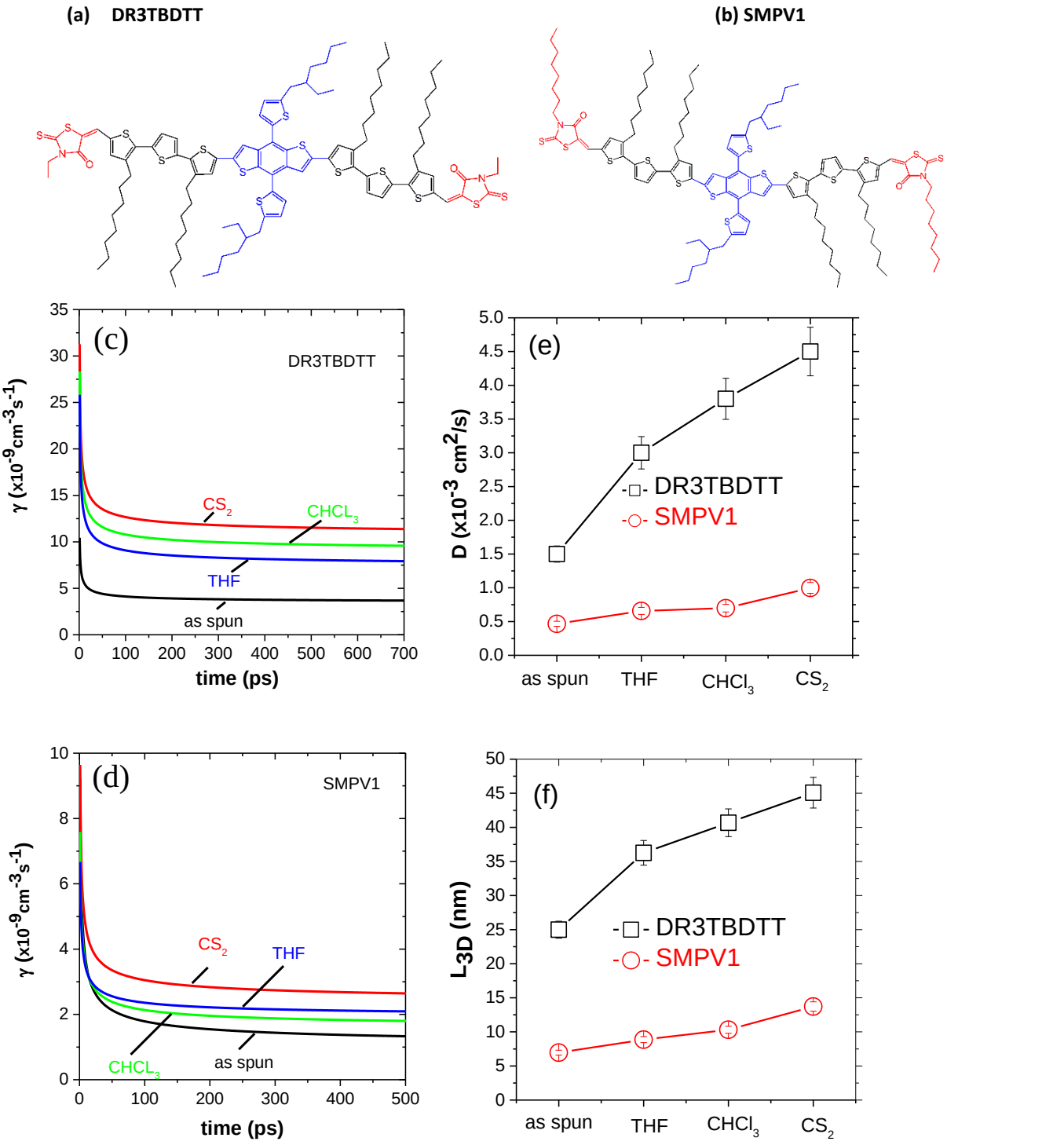

Fig. 1: Molecular structures of donor molecules DR3TBDTT and SMPV1 (a,b) and exciton diffusion measurements (c-f). Rate constant γ of singlet-singlet exciton annihilation (c,d) is obtained from intensity-dependent PL decays shown in Fig. S2 and S3 by fitting to Equation 1. The exciton diffusion coefficient D (e) and three-dimensional diffusion length L_{3D} (f) in the films annealed using different solvents were determined using Equations 2 and 3, respectively.

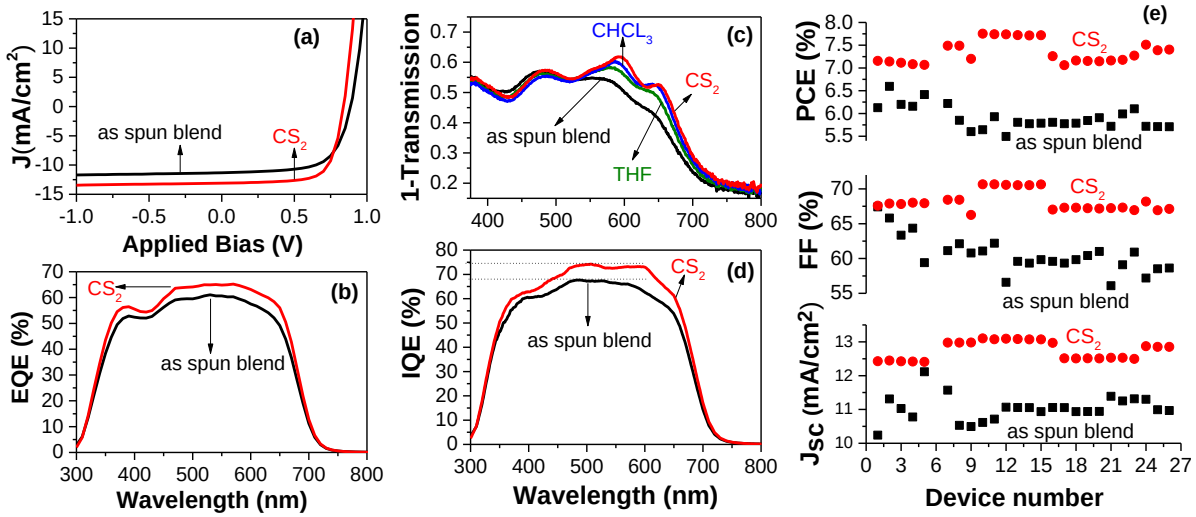

Fig. 2: Device characteristics of DR3TBDTT:$PC_{71}BM$ blend with and without CS_2 solvent vapour annealing: (a) Current density-voltage (J-V) curves. (b) External quantum efficiency (EQE). (c) Absorption spectra of blend films annealed using different solvents. (d) Internal quantum efficiency (IQE). (e) Short circuit current (J_{sc}), fill factor (FF) and power conversion efficiency (PCE) of devices with and without CS_2 SVA.

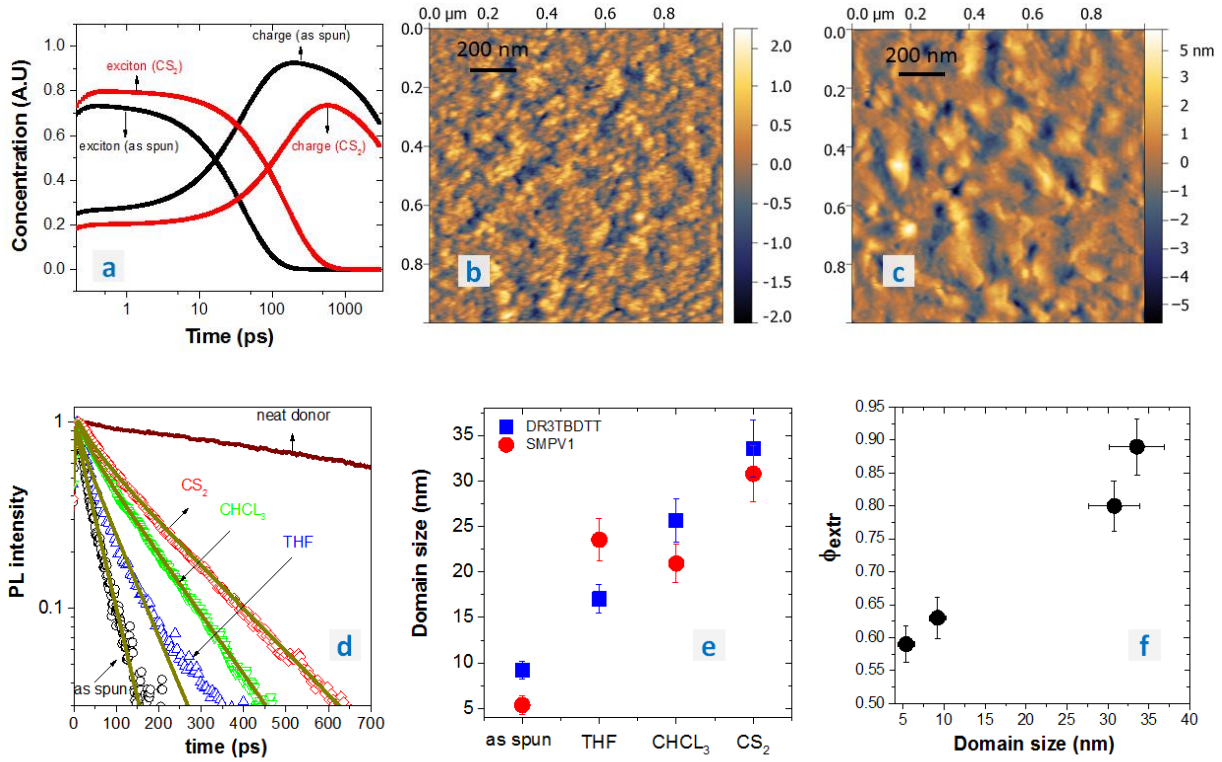

Fig. 3: (a) Dynamics of charge generation in DR3TBDTT: $PC_{71}BM$ blends obtained from TA spectra before and after solvent vapour annealing. AFM images of DR3TBDTT: $PC_{71}BM$ blend before (b) and after SVA in CS_2 (c) showing larger length scale of phase separation after SVA. (d) Time-resolved PL quenching of as-spun blend of DR3TBDTT with $PC_{71}BM$ before and after SVA in different solvents and PL decay in neat DR3TBDTT film. Solid lines are fits to the data using Equation S4. (e) Average domain sizes of $PC_{71}BM$ extracted from PL quenching data in blends with different donors. (f) Charge extraction efficiency as a function of average domain size.

Table 1. *Photovoltaic parameters of DR3TBDTT: $PC_{71}BM$ and SMPV1: $PC_{71}BM$ before and after solvent vapour annealing. IQE_{max} is maximum internal quantum efficiency, Φ_{gen} is charge generation efficiency and Φ_{extr} is charge extraction efficiency. For each case, the average parameters are given in the first row and the best device results in the second row.*

Molecules	IQE_{max} (%)	J_{sc} (mA/cm^2)	Voc (v)	FF (%)	PCE (%)	Φ_{gen}	Φ_{extr}
DR3TBDTT (untreated)	68	11.0 ± 0.4	0.885 ± 0.006	60.5 ± 2.6	5.91 ± 0.26	0.93	0.63
Best		11.3	0.886	65.8	6.59		
DR3TBDTT (CS_2 treated)	75	12.8 ± 0.3	0.845 ± 0.009	68.2 ± 1.5	7.35 ± 0.25	0.74	0.89
Best		13.1	0.837	70.7	7.75		
SMPV1 (untreated)	60	10.3 ± 0.6	0.918 ± 0.005	65.0 ± 2.7	6.17 ± 0.33	0.88	0.59
Best		10.6	0.918	67.7	6.60		
SMPV1 (CS_2 treated)	64	10.8 ± 0.3	0.887 ± 0.013	68.7 ± 1.9	6.61 ± 0.31	0.71	0.80
Best		11.4	0.888	70.5	7.13		

Journal Name

Full Paper